Spin dynamics in the quantum antiferromagnetic chain compound $KCuF_3$

S. E. Nagler,* D. A. Tennant, and R. A. Cowley
Clarendon Laboratory, Department of Physics, University of Oxford, Parks Road, Oxford, United Kingdom

T. G. Perring
Rutherford Appleton Laboratory, Chilton, Didcot, Oxon, United Kingdom

S. K. Satija
National Institute of Standards and Technology, Gaithersburg, Maryland 20899
(Received 11 June 1991)

The magnetic excitations of a nearly ideal realization of a one-dimensional $S=\frac{1}{2}$ Heisenberg antiferromagnet, $KCuF_3$, have been studied by inelastic neutron scattering. The experimments were performed using the pulsed neutron source ISIS and show that the magnetic scattering occurs at energies well above the top of the linearized spin-wave band. This result shows that it is essential to take account of quantum effects in discussing the excitations. The results are in excellent accord with theoretical predictions for the dynamical correlation function.

I. INTRODUCTION

Quantum effects give rise to many unusual phenomena in condensed-matter physics. They are particularly important in low-dimensional magnetic systems which may be disordered at all nonzero temperatures. Heisenberg antiferromagnetic chains have particularly interesting behavior. The excitation spectrum of chains with integer spin, S, exhibits the Haldane gap[1] even though no gap is given by ordinary spin-wave theory. In contrast, the spectrum for half-integer S is gapless, but for $S=\frac{1}{2}$ the excitations are not well-defined modes: For a given wave vector, Q, the spectrum is spread over a range of energies. This paper presents the results of an inelastic-neutron-scattering study of $KCuF_3$, a nearly ideal $S=\frac{1}{2}$ Heisenberg antiferromagnetic chain. As discussed below, the magnetic response arises from a continuum of excited states and is very different from the response of the corresponding classical system.

With the spins separated by a unit distance, the Hamiltonian of the model system can be written as

$$\hat{\mathcal{H}}=2J\sum_r \mathbf{S}_r\cdot\mathbf{S}_{r+1} . \tag{1}$$

The ground state for $S=\frac{1}{2}$ was first found by Bethe.[2] It is a singlet state, with no long-range antiferromagnetic order, and thus differs in a fundamental way from the Néel ground state of the corresponding classical model. Assuming the Néel state, a normal linear spin-wave analysis of the Hamiltonian leads to the dispersion relation

$$\omega_Q^{\rm cl}=2J|\sin(Q)| . \tag{2}$$

Experiments on linear-chain antiferromagnets with $S=\frac{5}{2}$, such as $(CD_3)_4NMnCl_3\cdot 2N(C_5D_5)$ (TMMC) are consistent with linear spin-wave theory.[3] For $S=\frac{1}{2}$, quantum effects are more important. Des Cloizeaux and Pearson[4] (dCP) showed that the lowest-lying excited states are given for wave vector Q as

$$\omega_Q^{\rm dCP}=\pi J|\sin(Q)| . \tag{3}$$

The dCP dispersion relation agrees with excitation energies observed by inelastic neutron scattering in the model one-dimensional (1D) systems $CuCl_2\cdot 2N(C_5D_5)$ (CPC) (Refs. 5 and 6) and $KCuF_3$.[7,8] The principal quantum effect would then seem to be a simple renormalization of the excitation spectrum by a factor of $\pi/2$.

In fact, the confirmation of the renormalization in real systems is not as straightforward as one might expect. Normal classical spin-wave theory also provides a totally self-consistent description of the experimental results. Since $\omega_Q^{\rm cl}$ and $\omega_Q^{\rm dCP}$ are identical apart from a constant factor of $\pi/2$, an independent measure of the exchange constant, J, is necessary to establish the validity of the dPC relation. If J is determined by fitting the measured static susceptibility[9] to that calculated for the $S=\frac{1}{2}$ chain,[10] the observed spin-wave frequencies are well fit by $\omega_Q^{\rm dCP}$. However, the susceptibility data can also be acceptably fitted[8] to the expression for the classical spin chain.[11] Carrying out this procedure for $KCuF_3$ or CPC yields a different value of J, the use of which allows the measured dispersion relations to be described precisely by $\omega_Q^{\rm cl}$.

Notwithstanding the ambiguity in the energy scale, the experimental results on CPC differ from linear spin-wave theory in an important way: careful measurements of the line shapes of the observed excitations[6] revealed that they are asymmetric with a high-energy tail. The measurements on $KCuF_3$ (Refs. 7 and 8) also show hints of this feature. This characteristic of the scattering arises from a purely quantum effect. Analytic calculations[12] and finite chain calculations[13] lead to the conclusion that the spectrum is a spin-wave continuum (SWC) of excitations, with the lower-energy bound ($\omega_Q^{\rm dCP}\equiv\omega_Q^{l}$) given by Eq.

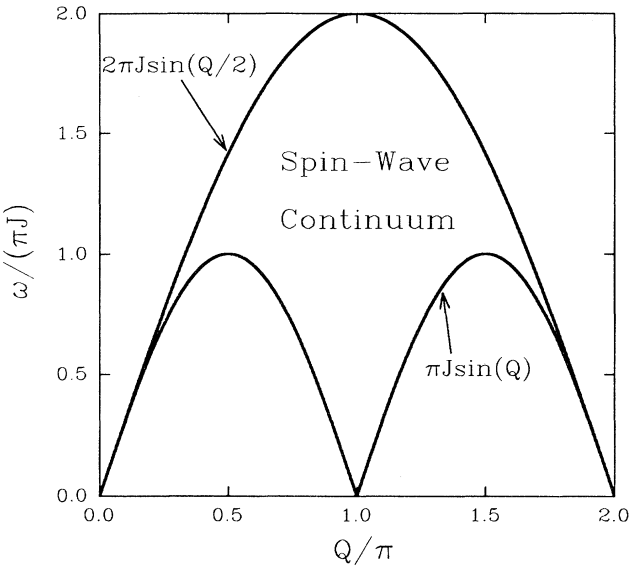

FIG. 1. The spin-wave continuum (SWC) spectrum of the spin-$\frac{1}{2}$ Heisenberg antiferromagnetic chain. The lower bound is the des Cloizeaux-Pearson dispersion relation.

(3), and the upper bound given by

$$\omega_Q^u = 2\pi J |\sin(Q/2)| \ . \tag{4}$$

The SWC spectrum is shown in Fig. 1. The wave vector $Q=\pi$ is the zone boundary (ZB), often termed the "antiferromagnetic zone center" in discussions of spin-wave excitations. One feature of the SWC is that it has a periodicity of 2π, the same as the underlying structural reciprocal lattice. Since the 1D system does not have antiferromagnetic long-range order, there is no reason for periodicity with $Q=\pi$ as manifested by $\omega_Q^{\rm cl}$ or $\omega_Q^{\rm dCP}$. The SWC extends to any energy that is double that of the $Q=\pi/2$ ["antiferromagnetic zone boundary" (AFZB)] spin wave. Classically, the frequency of the mode at the AFZB, $(\omega_{\pi/2})$, represents the largest energy contributing to the dynamic response at $T=0$. The presence of continuum scattering up to $\omega \approx 2\omega_{\pi/2}$ is an indication that the excitations from the quantum ground state are dominated by what would be described classically as interactions between the spin waves.

In this paper we present the results of a pulsed neutron-scattering study of the spin dynamics of the model system $KCuF_3$. The time-of-flight technique used has excellent energy resolution and inherently low background. As discussed below, this method has particular advantages for the study of excitations in low-dimensional systems. The rest of the paper is organized as follows: Section II discusses the dynamical correlation functions of the model system. In Sec. III the experimental technique is described in detail. The analysis of the results is presented in Sec. IV, a discussion in Sec. V, and the summary and conclusions in Sec. VI.

II. THEORY

For a quasi-one-dimensional system, the cross section for neutron scattering with momentum transfer **K** depends only on the component parallel to the chains, $K_\parallel \equiv Q$. For the Heisenberg chain, the magnetic scattering of unpolarized neutrons is proportional to the dynamical correlation function, given at $T=0$ as

$$S^{\alpha\alpha}(Q,\omega) = \sum_E |\langle E|S_Q^\alpha|G\rangle|^2 \delta(\omega - E) \ , \tag{5}$$

where S_Q^α is the Fourier-transformed spin operator of component $\alpha = x$ y, or z, $|G\rangle$ is the ground state with zero energy, and $|E\rangle$ is an eigenstate of the Hamiltonian with energy E. For classical spins aligned along the z direction, linear spin-wave theory[14] gives the transverse response

$$S^{xx}(Q,\omega) = S^{yy}(Q,\omega) = |\tan(Q/2)| \delta(\omega - \omega_Q^{\rm cl}) \ . \tag{6}$$

The longitudinal component $S^{zz}(Q,\omega)$ has a logarithmic singularity at $\omega_Q^{\rm cl}$.

The classical theory starts from the premise that the ground state is the Néel state, in which the sublattice magnetization has long-range order. For the quantum chain, the long-range order is absent, so the transverse and longitudinal components cannot be defined, and all of the components of $S^{\alpha\alpha}(Q,\omega)$ are identical. Although exact solutions exist for the ground state and low-lying eigenstates of the $S=\frac{1}{2}$ chain, they are too complicated to allow for an analytic calculation of the relevant matrix elements. There is not yet an exact solution for these correlation functions.

Many of the existing theoretical results for the correlation functions have been summarized in an important paper by Müller *et al.*[15] In the small-Q limit (or $Q \approx 2n\pi$) sum-rule calculations[16] show that the response is dominated by the dCP mode. On the other hand, an expansion in the parameter $1/S$,[17] valid when $Q \approx \pi$, shows a high-frequency tail in $S^{\alpha\alpha}(Q,\omega)$. Unfortunately, the expansion is least valid for $S=\frac{1}{2}$, where the tail is most important. Guided by exact results for the one-dimensional XY model,[18] numerical calculations of finite-spin chains, and known sum rules, Müller *et al.*[15] constructed an ansatz for the correlation function of the $S=\frac{1}{2}$ chain at $T=0$

$$S^{\alpha\alpha}(Q,\omega) = \frac{1}{\sqrt{\omega^2 - (\omega_Q^l)^2}} \Theta(\omega - \omega_Q^l)\Theta(\omega_Q^u - \omega) \ , \tag{7}$$

where $\Theta(\omega)=1$ if $\omega > 0$, and 0 otherwise, and ω_Q^l, ω_Q^u are the lower and upper bounds of the SWC. This form for $S^{\alpha\alpha}(Q,\omega)$ exhibits a square-root singularity at the lower bound. It gives reasonable results (to order unity) for known sum rules for the correlation functions. Taking into account numerical resolution, Eq. (7) is consistent with recent quantum Monte Carlo calculations.[19] Even though the abrupt cutoff at the high-frequency end is probably unphysical, it represents the best available reasonable analytic expression for $S(Q,\omega)$ of the 1D Heisenberg antiferromagnet.

III. EXPERIMENTAL DETAILS

The structure of $KCuF_3$ is tetragonal with lattice parameters at 10 K of $a=b=4.126$ Å, and $c=3.914$ Å.[8]

The magnetic chains of Cu^{2+} ions run along the c axis. There are two polytype structures, denoted (a) and (b), corresponding to slightly different arrangements of the fluorine atoms.[20] Interchain interactions lead to a low-temperature magnetic structure with spins aligned ferromagnetically in the a-b plane and stacked antiferromagnetically along the c axis. The nominal transition temperatures to a 3D antiferromagnetically ordered state are $T_N \approx 39$ K for type (a), and $T_N \approx 22$ K for type (b).[21]

Satija *et al* [8] used conventional triple-axis inelastic neutron scattering to study a $KCuF_3$ crystal consisting of 99% of polytype (a). Their measurements of the spin-wave dispersion at low temperatures[7,8] established the following results: The ratio of the interchain and intrachain exchange interactions is $J_{\parallel}/J_{\perp} \approx 0.01$. The intrachain exchange can be thought of as purely isotropic (Heisenberg), with a small xy-like anisotropy of about 0.2%. The dispersion along the c axis fits the dCP spectrum very well with $J = 17.5$ meV, corresponding to an antiferromagnetic zone-boundary energy $\omega_{\pi/2} = 55.0$ meV. Dispersion perpendicular to the c axis is negligible for energy transfers above 15 meV. The results are consistent with those of Hutchings *et al.*[7]

The crystal used in the present study was the same one used earlier by Satija *et al.*[8] It has a volume of approximately 1 cm^3. A small fraction ($\approx 1\%$) of the sample was a second crystallite, misoriented with respect to the main part of the sample by a nearly 90° rotation about the b axis. The crystal was mounted in a He-gas-filled aluminum can with Cd foil wrapped around the extremities of the mount. The mounted sample was placed in a cryostat at the position of the center of rotation of the Multi Angle Rotor Instrument (MARI) at the ISIS pulsed neutron source. The temperature could be controlled to within 0.1 K or better over several days.

Neutrons produced by spallation were moderated by a methane moderator, and monochromated by a Fermi chopper, producing a beam with incident energy, E_0, variable from 20 to 2000 meV, and intrinsic resolution equal to roughly 1% of E_0. The fast neutron background was reduced with a nemonic chopper, and the incident beam intensity measured with monitor counters before and after the monochromator. The scattered neutrons were detected in an array of high-pressure helium detectors located 4 m from the sample position. The low-angle array consisted of eight banks arranged symmetrically about the direction of the incident neutron beam. The scattering angles covered in the low-angle array range from $\phi = 3.86°$ to $\phi = 12.0°$. For this experiment a total of 109 detectors were used in the low-angle array. Data were also collected in the high-angle detector array extending up to $\phi = 135°$. The detector efficiencies and solid-angle coverage were normalized by measuring the scattering from a standard vanadium specimen.

The $KCuF_3$ crystal was aligned so that the $(h,0,l)$ plane coincided with the horizontal. Rotation about the vertical axis allowed any reciprocal-lattice vector in this plane to be lined up parallel to $\mathbf{k}_0$, the wave vector of the incident neutrons. The one-dimensional magnetic scattering depends on the c^* component of momentum transfer only. Therefore, with the $(0,0,l)$ direction aligned along $\mathbf{k}_0$, all detectors at fixed ϕ have identical magnetic scattering, and can be summed with no loss of information. The consequent improvement in statistics provides a large advantage for the study of quasi-one-dimensional systems.

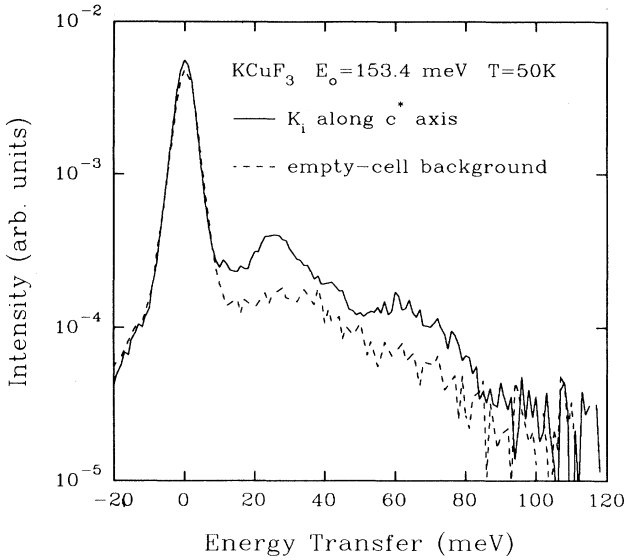

FIG. 2. Raw data obtained with $\mathbf{k}_0$ along $\mathbf{c}^*$, $E_0 = 153.4$ meV, and a temperature $T = 50$ K, superposed on the empty-cell background measured with the same incident energy. The scattering has been normalized by the incident neutron flux.

The scattering was measured for several different values of E_0, probing different regions of the magnetic response. Measurements were made with $\mathbf{k}_0$ parallel to both the $\mathbf{c}^*$ and $\mathbf{a}^*$ axes, and also of the empty-cell scattering, with conditions being identical except for the absence of the $KCuF_3$ crystal. For most of the runs the temperature was set to 50 K, assuring that 3D effects played a minimal role in the observed scattering. Figure 2 shows typical "raw data" for a scan with $\mathbf{k}_0$ aligned along $\mathbf{c}^*$ superposed on an empty-cell run. The data are acquired in a "time-of-flight" mode, and the conversion the measured cross section into a cross section per unit frequency is accompanied by a subtraction of a well-characterized time-modulated background. The data represent the sum of all the scattering in the eightfold symmetric low-angle bank, normalized by the monitor counts and corrected for detector efficiency and solid angle using white beam and monochromatic vanadium spectra. The data have also been corrected for the kinematic factor k_f/k_0 to obtain the correlation functions.

In order to interpret the data it was necessary to establish the nonmagnetic background scattering. The empty-cell runs were dominated by scattering from the density of states of Al and multiphonon scattering, both of which were observed to be isotropic. To assess the additional background arising from the sample, data was accumulated with $\mathbf{k}_0$ aligned along $\boldsymbol{\alpha}^*$. In this geometry the momentum transfer of neutrons detected in the two vertical detector banks has essentially no component of

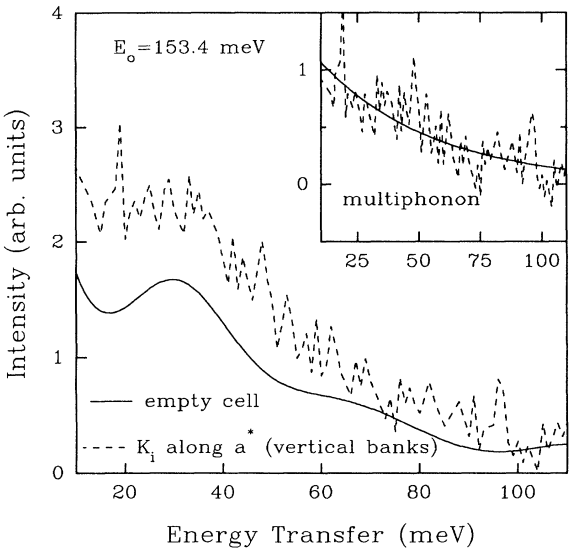

FIG. 3. Sum of scattering in the vertical low-angle detector banks, with $\mathbf{k}_0$ along $\mathbf{a}^*$, $E_0=153.4$ meV, and $T=50$ K, superposed on the smoothed empty-cell scattering, normalized by neutron flux, and vanadium runs (see text). Inset: the difference scattering fitted to a simple exponential.

$\mathbf{c}^*$, and therefore represents magnetic scattering from $Q=0$, which has vanishing intensity for an antiferromagnet. The scattering measured in this way is shown in Fig. 3, along with a smooth curve fitted to the empty-cell data. The empty-cell data come from the sum of scattering in all eight of the low-angle arrays, while the scattering from the sample is the sum of the two vertical banks only. The two can be compared directly by using scattering from vanadium standards to account for differences in detector efficiency and solid-angle coverage, and normalizing by the incident neutron flux. The inset shows the scattering with the empty-cell contribution subtracted. The result is a monotonically decreasing function of energy transfer. This represents the multiphonon scattering from the sample alone. The solid line is a fit to a simple decaying exponential, which is what one expects in a simplified diffusive model of multiphonon scattering.[22] In general, the relative importance of multiphonon scattering increases with incident neutron energy. The multiphonon scattering is usually a smoother function of energy transfer than scattering arising from the phonon density of states or individual modes. Consequently, as the incident neutron energy is increased, one expects the overall nonmagnetic background to be higher and smoother. It should be noted that the high-angle detector banks measure scattering with larger momentum transfers, which is dominated by phonon scattering. Comparison of the low- and high-angle detector banks confirms that the background arises from phonon scattering. If it is assumed that the multiphonon scattering from the sample is isotropic, the scattering in the low-angle vertical banks with $\mathbf{k}_0$ parallel to $\boldsymbol{\alpha}^*$ can be taken as a direct measure of the background, and, after proper normalization, simply subtracted from the scattering measured with $\mathbf{k}_0$ along $\mathbf{c}^*$ to obtain the magnetic scattering.

IV. ANALYSIS

The observed magnetic scattering can be compared with a theoretical model such as Eq. (7) if the instrumental resolution is known. The major contribution to the resolution arises from the summing over many detectors, and this smears the momentum transfer resolution. Another contribution arises from the bandpass of the Fermi chopper and time-of-flight measurement. This contribution dominated the uncertainty in energy transfer. The wave vector effect is discussed first. Consider a neutron of initial momentum $\mathbf{k}_0$, and energy $E_0=\gamma^{-1}k_0^2$, scattered with final momentum and energy $\mathbf{k}_f$, E_f, into a detector at a scattering angle ϕ from the incident direction. Defining the momentum transfer $\mathbf{K}=\mathbf{k}_0-\mathbf{k}_f$, and energy transfer $\omega=E_0-E_f$, one can write

$$\mathbf{K}=\mathbf{Q}_{\parallel}+\mathbf{Q}_{\perp}\ , \tag{8}$$

where

$$Q_{\parallel}=k_0-k_f\cos\phi\ , \tag{9}$$

$$Q_{\perp}=k_f\sin\phi\ . \tag{10}$$

The component of momentum transfer along the incident direction can be determined as a function of the incident energy, scattering angle, and energy transfer:

$$Q_{\parallel}^2(E_0,\phi,\omega)=\gamma[E_0(1+\cos^2\phi-2\cos\phi\sqrt{1-\omega/E_0}$$

$$-\omega\cos^2\phi] \tag{11}$$

The constant $\gamma=0.4826\ \text{Å}^{-2}\,\text{meV}^{-1}$.

When $\mathbf{k}_0$ lies along $\mathbf{c}^*$, Eq. (12) defines the locus of an individual detector's scan at fixed E_0. An example is shown in Fig. 4(a) where, for $E_0=153.4$ meV, the energy transfer is shown against the one-dimensional momentum transfer $Q=Q_{\parallel}c/2$. The SWC spectrum is plotted in the extended zone scheme. The upper and lower lines represent detectors at the minimum and maximum values of scattering angle present in the low-angle bank. When a scan is summed over the low-angle bank, there will be contributions from the range between the two lines. From this diagram it is possible to infer instantly where possible contributions to the magnetic scattering may occur. In a classical model, a sharp peak is expected when the locus crosses the lower bound ($\omega_Q^{\rm dCP}$ or $\omega_Q^{\rm cl}$). On the other hand, if all of the states of the SWC contribute, there will be scattering whenever the locus lies within the continuum. The energy resolution may be approximated by a Gaussian with the full width half maximum (FWHM) uniquely determined by the ratio ω/E_0.[22] In practice, the FWHM is of the order of 1% of E_0. Under the assumption that all of the momentum transfer uncertainty is accounted for by kinematic effects, the expected magnetic scattering intensity for the quasi-1D antifer-

romagnet with $\mathbf{k}_0 \| \mathbf{c}^*$ may be written as

$$I(E_0,\omega) = A \sum_{\phi} g(\phi) \left[\int R(\omega-\omega') |f[K(E_0,\phi,\omega')]|^2 \times S^{xx}[Q(E_0,\phi,\omega'),\omega'] d\omega' \right], \tag{12}$$

where A is an overall constant, g is the number of detectors at scattering angle ϕ, R is the energy resolution function, f the magnetic form factor, and $S^{xx}(Q,\omega)$ the dynamical correlation function. The kinematical factor k_f/k_0 is suppressed as it is accounted for in the normalization of the data. As written, Eq. (12) assumes that $S^{\alpha\alpha}(Q,\omega)$ is identical for $\alpha = x$, y, or z. This is true for Eq. (7), but if, for example, linear spin-wave theory is assumed, and, as in the 3D ordered state, all spins are perpendicular to the c axis, then one must insert a polarization factor.[23]

Figure 4(b) shows the calculated intensity corresponding to the scan depicted in Fig. 4(a). The quantum calculation used Eq. (7) while the classical calculation uses Eq. (6) and the appropriate polarization factor assuming that all of the spin-wave scattering is transverse. The value of the exchange constant used in the classical calculation is chosen so that the classical dispersion coincides with the lower bound of the SWC. In both cases an analytic approximation for the $\langle j_0 \rangle$ form factor for Cu^{2+} has been used.[24] The linear spin-wave calculation has been shown to give accurate peak positions, line shapes, and relative intensities for the classical $S = \frac{5}{2}$ antiferromagnetic chain system $KFeS_2$.[25,26] In the case of $KCuF_3$ several differences between the scattering of the classical and quantum models are clear. The most striking contrast is the presence, within the quantum model, of a broad feature at energies above 55 meV, the spin-wave energy at $Q = \pi/2$. This feature does not appear at all in the classical model, and corresponds to the locus of the scan cutting through the continuum in a region above the maximum of the dCP band. Where scattering occurs in both models, the quantum response shows a single broad feature near the point $Q = \pi (\omega \approx 25$ meV), where, in fact, the classical model shows two well-resolved peaks. In both models the feature around 45 meV, which corresponds to $Q \approx 2\pi$, is a relatively sharp peak. The classical model, however, predicts a larger difference in intensity

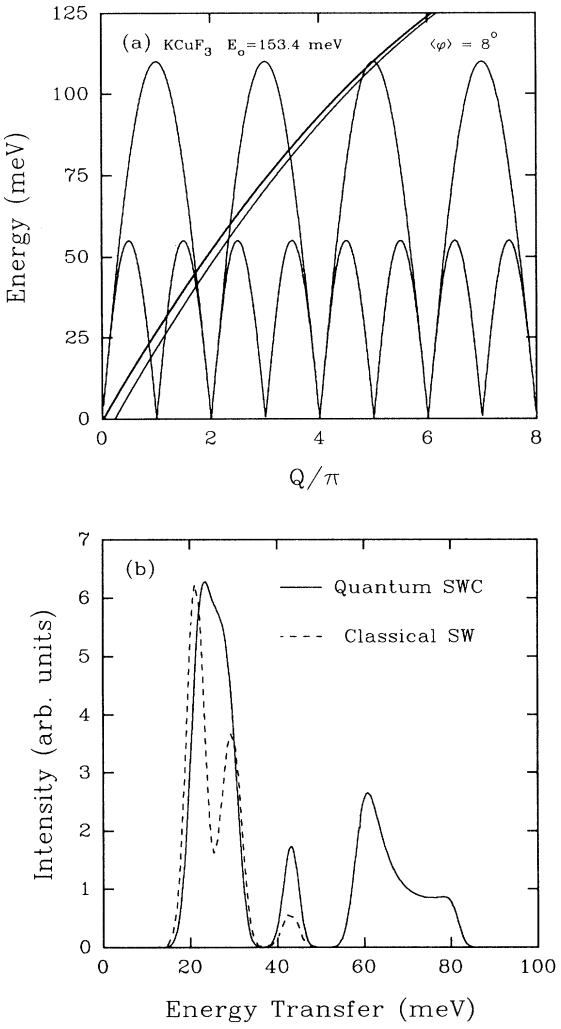

FIG. 4. (a) Locus of a scan with $E_0 = 153.4$ meV, assuming that $\mathbf{k}_0 \| \mathbf{c}^*$. The upper and lower lines of the locus correspond to detectors at $\phi = 3.9°$ and $\phi = 12°$, respectively. (The average scattering angle in the low-angle bank is $\langle \phi \rangle = 8°$.) The upper and lower bounds of the SWC (see text) have been plotted in the extended zone scheme. (b) Calculated intensity of magnetic scattering corresponding to the scan shown in (a). The calculation is done for both the quantum and classical expressions for $S(Q,\omega)$, and includes instrumental resolution effects as discussed in the text.

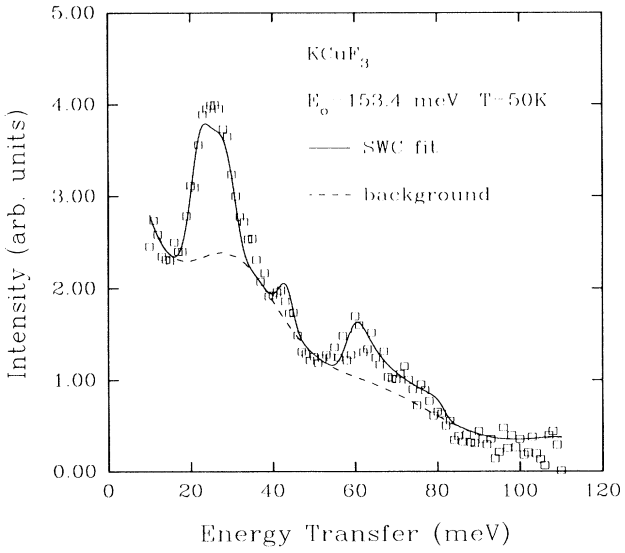

FIG. 5. Scan with $\mathbf{k}_0 \| \mathbf{c}^*$, and $E_0 = 153.4$ meV. The data are grouped into 1-meV bins. The dashed line represents the nonmagnetic background. The solid line is a model fit as described in the text.

between the antiferromagnetic ($Q=\pi$) and nuclear zone centers. These general features are present for $E_0 \approx 100-200$ meV, although the details of the line shapes depend on the incident energy.

At temperatures greater than $T_N=38$ K, it is reasonable to assume that $KCuF_3$ behaves like an ideal one-dimensional system and apply Eqs. (11) and (12) to the analysis of the data. Figure 5 shows a scan at a sample temperature of 50 K with $E_0=153.4$ meV and $\mathbf{k}_0 \| \mathbf{c}^*$. The data were collected in approximately 10 h. The scan corresponds directly to that illustrated in Fig. 4. The data have been binned into 1-meV units for clarity of presentation. The dashed line represents a smooth function fit to the nonmagnetic background as determined above. The solid line is a fit to a sum of the nonmagnetic background plus a constant times the scattering calculated from the quantum model. The values of the lattice parameter, c, and exchange constant J, were fixed; J being obtained from the previous triple-axis study.[8] Therefore, the only adjustable parameter is the overall constant A in Eq. (12). For $S(Q,\omega)$, expression (7) of Müller *et al.*[15] has been used, multiplied by a Bose temperature factor $n_\omega+1$ to ensure detailed balance. The temperature factor is probably not necessary, as the ratio of thermal energy (T/k_B) to πJ is only 0.07, and comparing the calculation to that for $T=0$ shows that the change in relative intensity at different energies is less than 1% across the measured range.

The overall fit is excellent. The three main features in the calculated scattering illustrated in Fig. 4 are all present. The observed line shapes are well described by the theory. The fit somewhat underestimates the observed intensity difference in the 25- and 45-meV features. The sum of squared deviations normalized by the degrees of freedom is $\chi^2=1.46$. Most of the background is from the empty cell, but there is a contribution from multiphonon scattering in the sample as described above. If the background contribution from the sample is allowed to vary in amplitude and width, the resulting $\chi^2=1.32$ is a slight improvement, but the quality of the fit as seen "by eye" is not substantially better. This procedure might be justified as an attempt to account for possible anisotropy in the multiphonon scattering from the sample.

Figure 6 shows a similar scan with $E_0=204.8$ meV. As an illustration, the fit plotted is that where the extra parameters describing the sample-dependent multiphonon scattering have been allowed to vary, giving $\chi^2=1.31$. An acceptable fit is also obtained if these parameters are fixed. As for the 153.4 meV scan, the overall fit is excellent, but the intensity of the scattering from the magnetic zone center ($Q=\pi$, $\omega \approx 30$ meV) is slightly underestimated relative to that at the nuclear zone center ($Q=2\pi$, $\omega \approx 50$ meV).

A further scan with $E_0=102.0$ meV is shown in Fig. 7. The background scan for this incident energy was not correctly acquired as $\mathbf{k}_0$ was misaligned relative to $\mathbf{a}^*$. It was therefore *necessary* to fit the total scattering with additional parameters in order to estimate the contribution of the sample to the nonmagnetic background. This was complicated by the fact that the empty-cell scattering has structure in the vicinity of the one of the magnetic features. The determination of the background for the $E_0=102.0$ scan was therefore less reliable than for the other incident energies measured. In any case, the fit is still obviously acceptable, with the major characteristics similar to the other scans.

With proper normalization for the incident neutron flux, the fitted constant "A" should, in principle, be independent of incident energy. The random fitting uncer-

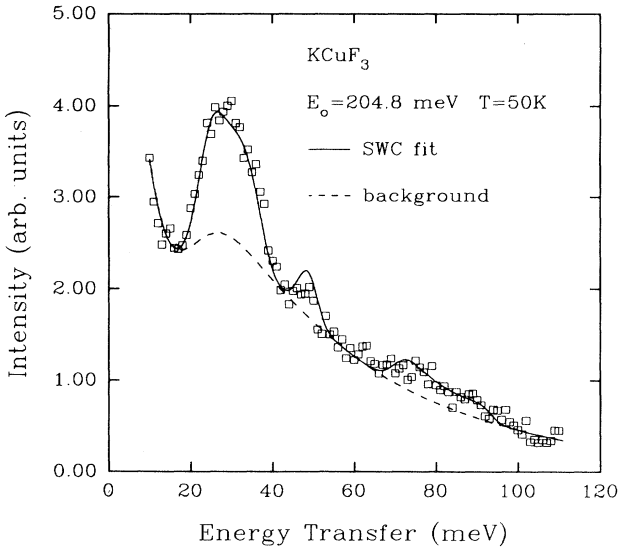

FIG. 6. Scan with $\mathbf{k}_0 \| \mathbf{c}^*$, and $E_0=204.8$ meV. The data are grouped into 1-meV bins. The dashed line represents the nonmagnetic background. The solid line is a model fit as described in the text.

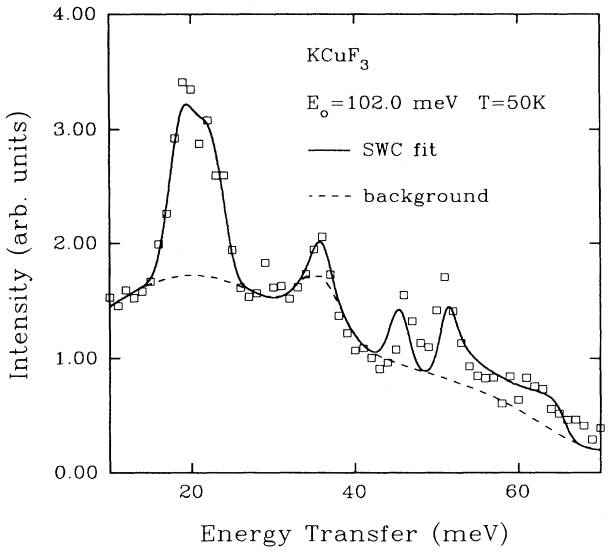

FIG. 7. Scan with $\mathbf{k}_0 \| \mathbf{c}^*$, and $E_0=102.0$ meV. The data are grouped into 1-meV binds. The dashed line represents the nonmagnetic background. The solid line is a model fit as described in the text.

tainties alone are of the order of 5%. Defining the fitted constant $A(153.4\ \text{meV})=1.00$, the other two values are $(102.0)=0.84$, $A(204.8)=1.07$. The values for 204 and 153 meV are equal within experimental accuracy. The constant for 102 meV differs by about 15%, but there may be a sizable systematic error arising from the background determination problems.

V. DISCUSSION

The background subtracted magnetic scattering for $E_0=153.4$ meV is shown in Fig. 8. The representative error bars are 1σ including statistical errors only, and have *not* been increased to account for the effect of subtracting the background. The solid line shows the SWC fit described above. The corresponding plot for $E_0=204.8$ meV is given in Fig. 9 and that for $E_0=102.0$ meV in Fig. 10.

In order to test whether a modified version of linear spin-wave theory can describe the data, a fit was also carried out to a spin-wave model with Lorentzian peaks of a variable linewidth. Since the major features unaccounted for by a simple spin-wave model are at high frequencies, and will be dominated by the width of the mode at the AFZB, the only additional fitting parameter is a constant linewidth for the mode. The resulting fit for $E_0=153.4$ meV is shown as a dashed line in Fig. 8. The conclusion is that a renormalization or simple modification of classical linear spin-wave theory is incapable of describing the observed scattering, which extends up to frequencies of the order of $2\pi J$. The high-frequency broad feature is a clear and unique signature of the quantum spin-excitation spectrum. The instrumental resolution prevents a direct measurement of any possible sharp energy cutoff of $S^{\alpha\alpha}(Q,\omega)$. Even so, the fact that the theory described the overall shape of this part of the scattering so well confirms that, even if there is no abrupt cutoff of

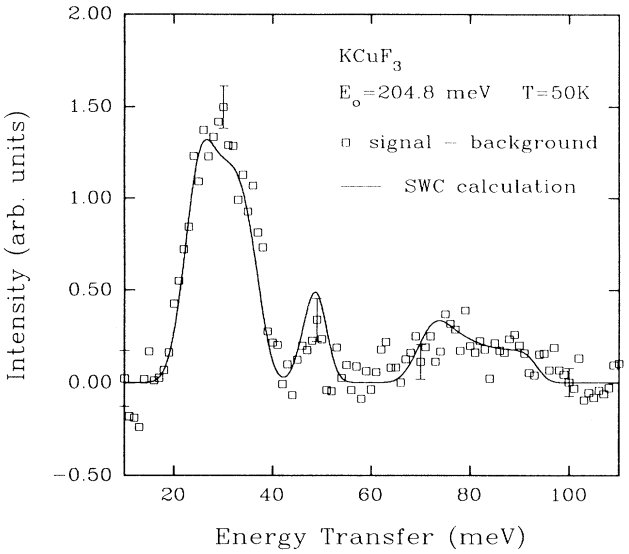

FIG. 9. The scan with $E_0=204.8$ meV, $\mathbf{k}_0\|\mathbf{c}^*$, with the smoothed nonmagnetic background subtracted. The representative 1σ error bars are statistical only, and are not adjusted to account for the background subtraction. This solid line is the fitted quantum $S(Q,\omega)$.

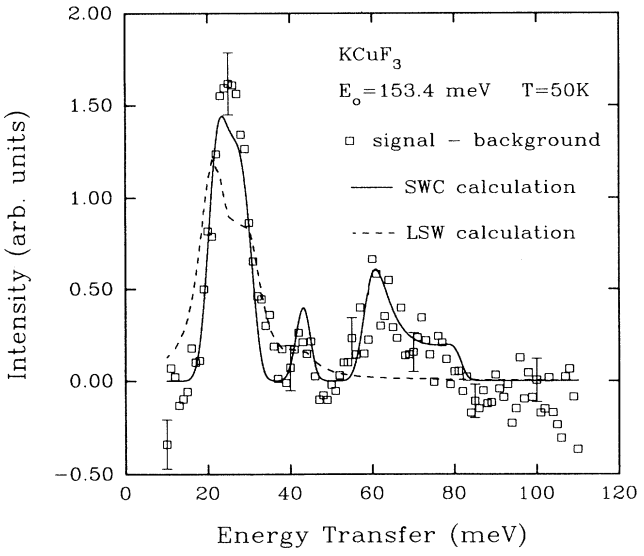

FIG. 8. The scan with $E_0=153.4$ meV, $\mathbf{k}_0\|\mathbf{c}^*$, with the smoothed nonmagnetic background subtracted. The representative one-standard-deviation (1σ) error bars are statistical only, and are not adjusted to account for the background subtraction. The solid line is the fitted quantum $S(Q,\omega)$. The dashed line is an attempt to fit to a modified spin-wave theory, as described in the text.

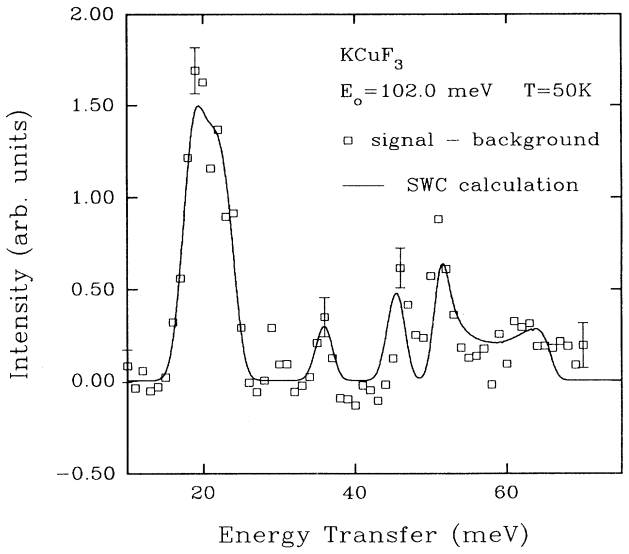

FIG. 10. The scan with $E_0=102.0$ meV, $\mathbf{k}_0\|\mathbf{c}^*$, with the smoothed nonmagnetic background subtracted. The representative 1σ error bars are statistical only, and are not adjusted to account for the background subtraction. The solid line is the fitted quantum $S(Q,\omega)$.

$S^{\alpha\alpha}(Q,\omega)$ at ω_Q^u, the bounds of the SWC do define the states giving rise to magnetic scattering.

The theory's small but systematic underestimation of the relative spectral weight near $Q=\pi$ requires careful consideration. One possibility is that the differences are due to the misaligned portion of the crystal, but this does not seem likely given the systematic nature and magnitude of the effect. The hypothetical form of $S(Q,\omega)$ does not satisfy sum rules exactly, and, in fact, is known to exclude contributions from a "triplet sea" of states that are important near $Q=\pi$, but at energies greater than $2\pi J$.[15] This does not explain the additional intensity seen experimentally, which is around 20–30 meV for the incident energies measured. Another possibility is that, even at 50 K, there are still residual 3D interactions. The effect on the incipient 1D spectrum is similar to the effect of a staggered field, possibly introducing a tendency to a more Néel-like ground state. For $S=\frac{1}{2}$ Ising-like materials, which also display an excitation continuum (albeit in a different manner), 3D effects are known to enhance the spectral weight at the lower bound of the continuum.[27] This interpretation is not strongly supported by preliminary measurements in $KCuF_3$ at 20 and 77 K, which appear to be substantially similar to the 50 K results reported in depth here. The detailed temperature dependence of the scattering is the subject of ongoing investigations.

VI. SUMMARY AND CONCLUSIONS

In this study we have used pulsed neutron scattering to investigate the magnetic excitation spectrum in the quasi-one-dimensional antiferromagnet $KCuF_3$. Our results demonstrate the effectiveness of the time-of-flight technique for measurements in low-dimensional systems. The presence of a quantum spin-excitation spectrum extending up to energies of the order of $2\pi J$ has been clearly established. Finally, the ansatz for $S(Q,\omega)$ proposed by Müller *et al.* provides an excellent description of the observed scattering. The detailed nature of the temperature dependence of the response will require further study.

ACKNOWLEDGMENTS

We have benefited from helpful discussions with S. E. Brown, J. Boncella, R. Osborn, D. F. McMorrow, and especially, R. A. Robinson. We would also like to express our gratitude to the staff at the R.A.L., notably Z. Bowden for expert technical assistance and M. Arai and A. D. Taylor for aid in running the spectrometer. Financial support was provided by the Science and Engineering Research Council, and one of us (S.E.N.) received additional support from the National Science Foundation under Award No. INT-8922482.

*Permanent address: Department of Physics, University of Florida, Gainesville, Florida 32611.

[1]F. D. M. Haldane, Phys. Rev. Lett. **50**, 1153 (1983).
[2]H. A. Bethe, Z. Phys. **71**, 205 (1931).
[3]M. T. Hutchings, G. Shirane, R. J. Birgeneau, and S. L. Holt, Phys. Rev. B **5**, 1999 (1972).
[4]J. des Cloizeaux and J. J. Pearson, Phys. Rev. **128**, 2131 (1962).
[5]Y. Endoh, G. Shirane, R. J. Birgeneau, P. M. Richards, and S. L. Holt, Phys. Rev. Lett. **32**, 170 (1974).
[6]I. U. Heilmann, G. Shirane, Y. Endoh, R. J. Birgeneau, and S. L. Holt, Phys. Rev. B **18**, 3530 (1978).
[7]M. T. Hutchings, H. Ikeda, and J. M. Milne, J. Phys. C **12**, L739 (1979).
[8]S. K. Satija, J. D. Axe, G. Shirane, H. Yoshizawa, and K. Hirakawa, Phys. Rev. B **21**, 2001 (1980).
[9]K. Hirakawa and Y. Kurogi, Prog. Theor. Phys. S **46**, 147 (1970).
[10]J. C. Bonner and M. E. Fisher, Phys. Rev. **135**, A640 (1964).
[11]M. E. Fisher, Am. J. Phys. **32**, 343 (1964).
[12]T. Yamada, Prog. Theor. Phys. **41**, 880 (1969).
[13]J. C. Bonner, B. Sutherland, and P. M. Richards, *Magnetism and Magnetic Materials-1974 (San Francisco),* Proceedings of the 20th Annual Conference on Magnetism and Magnetic Materials, AIP Conf. Proc No. 24, edited by C. D. Graham, G. H. Lander, and J. J. Rhyne (AIP, New York, 1975).
[14]P. W. Anderson, Phys. Rev. **86**, 694 (1952).
[15]G. Müller, H. Thomas, H. Beck, and J. C. Bonner, Phys. Rev. B **24**, 1429 (1981).
[16]P. C. Hohenberg and W. F. Brinkman, Phys. Rev. B **10**, 128 (1974).
[17]H. J. Mikeska, Phys. Rev. B **12**, 2794 (1975).
[18]Th. Niemeijer, Physica **36**, 377 (1967).
[19]J. Deisz, M. Jarrell, and D. L. Cox, Phys. Rev. B **42**, 4869 (1990).
[20]A. Ozaki, J. Phys. Soc. Jpn. **26**, 870 (1969).
[21]M. T. Hutchings, E. J. Samuelsen, G. Shirane, and K. Hirakawa, Phys. Rev. **188**, 919 (1969).
[22]T. G. Perring, PhD. thesis, Cambridge University, 1991.
[23]See, for example, W. Marshall and S. W. Lovesey, *Theory of Thermal Neutron Scattering* (Clarendon, Oxford, 1971).
[24]P. J. Brown (unpublished).
[25]D. Welz and M. Arai (unpublished).
[26]S. E. Nagler (unpublished).
[27]S. E. Nagler, W. J. L. Buyers, R. L. Armstrong, and B. Briat, Phys. Rev. B **27**, 1784 (1983).